Marine and Petroleum Geology 134 (2021) 105333

Contents lists available at ScienceDirect

Marine and Petroleum Geology

journal homepage: www.elsevier.com/locate/marpetgeo

Effects of upstream conditions on digitate shallow-water delta morphology

Zhenhua Xu [a,b], Shenghe Wu [a,b,*], Dali Yue [a,b], Junshou Zhao [c], Meng Deng [c], Zhao Liu [a,b], Jiajia Zhang [a,b], Mingcheng Liu [a,b], Wenjie Feng [d]

[a] State Key Laboratory of Petroleum Resources and Prospecting, China University of Petroleum-Beijing, Beijing, 102249, China
[b] College of Geosciences, China University of Petroleum-Beijing, Changping, Beijing, 102249, China
[c] Bohai Petroleum Research Institute, CNOOC Tianjin Branch, Tianjin, 300459, China
[d] School of Geosciences, Yangtze University, Wuhan, 430100, China

ARTICLE INFO

Keywords:
Digitate shallow-water delta
Bar finger
Morphology
Upstream conditions
Delft3D simulation

ABSTRACT

Digitate deltas consist of one or multiple separate bar fingers, which can form hydrocarbon reservoirs after burial. This paper focuses on digitate shallow-water deltas, which are commonly seen in modern and ancient deposits with similar downstream conditions. Four metrics were adopted to quantify their morphologies, including the average sinuosity, average nondimensional width (average width ratio between the bar fingers and distributary channels), nondimensional delta length (ratio between the delta length and average width of the distributary channels), and number of bar fingers. These metrics measured from 9 modern deposits and 21 Delft3D simulations exhibited wide-ranging values that were strongly affected by the upstream conditions. However, the effects of the upstream conditions remain unclear. The quantitative effects were revealed by performing Delft3D simulations: (1) the average sinuosity is proportional to the sediment cohesion and concentration and inversely proportional to the sand proportion and water discharge, and reaches equilibrium as sediment supply increases; (2) the average nondimensional width is proportional to the sediment concentration, is inversely proportional to the sediment cohesion and water discharge, has an inverse exponential relationship with the sand proportion, and is independent of the sediment supply; (3) the nondimensional delta length has a power-law relationship with the water discharge and is logarithmically related to the sediment supply; (4) the number of bar fingers is proportional to the sand proportion and sediment supply and inversely proportional to the sediment cohesion. Upstream conditions influence channel, mouth bar and levee growth, resulting in various bar finger morphologies. Empirical equations from Delft3D simulations were proven effective in examinations of nine modern deposits and applied to help predict the distribution of a digitate shallow-water delta reservoir. This work improves the fundamental understanding of the upstream controls in digitate shallow-water deltas and may help enhance the inter-well prediction of paralic reservoirs.

1. Introduction

Fluvial-dominated deltas can be divided into lobate and digitate deltas (Bernard, 1965; Fisher et al., 1969; Olariu and Bhattacharya, 2006; Burpee et al., 2015; Marfai et al., 2016). Lobate deltas develop sheet mouth bars deposited in multiple coeval terminal distributary channels (Donaldson, 1966; Dumars, 2002; Olariu and Bhattacharya, 2006). In contrast, digitate deltas are characterized by one or multiple separate bar fingers and consist of coeval distributary channels, mouth bars, and levee complexes (Fisk, 1954, 1955, 1961, 1955; Donaldson, 1974; Galloway, 1975; Rowland et al., 2010; Falcini and Jerolmack, 2010). Examples include the modern Mississippi River Delta and Yellow River Delta (Figs. 1 and 2). Bar fingers are sand-rich deposits (FISK, 1961; Donaldson, 1974; Xu et al., 2019) and thus are potential petroliferous targets after burial.

Digitate deltas are more commonly formed in shallow-water basins (where the ratio of the distributary channel depth to the basinal water depth at the distributary mouth is greater than 1; Edmonds et al., 2011a; Wu et al., 2019) compared to deep-water basins, based on morphological observations of modern lakes and bays (Fig. 1) as well as ancient petroliferous basins (e.g., Ordos Basin: Hu et al., 2008; Bohai Bay Basin: Zhang et al., 2017; Xu et al., 2019). Digitate shallow-water deltas exhibit various bar finger morphologies (Fig. 1). It is significant for the prediction of petroliferous reservoirs to research further the morphological

* Corresponding author. State Key Laboratory of Petroleum Resources and Prospecting, China University of Petroleum-Beijing, Beijing, 102249, China.
E-mail address: reser@cup.edu.cn (S. Wu).

https://doi.org/10.1016/j.marpetgeo.2021.105333
Received 4 January 2021; Received in revised form 14 September 2021; Accepted 15 September 2021
Available online 16 September 2021

characteristics and controlling factors of digitate shallow-water deltas and their bar fingers.

The combined upstream and downstream conditions control the delta morphology: upstream controlling conditions include water and sediment discharge (Postma, 1990; Orton and Reading, 1993), sediment properties (Caldwell and Edmonds, 2014); downstream controlling conditions include tidal and wave energies (Caldwell et al., 2019; Piliouras and Kim, 2019; Nienhuis et al., 2020), and basinal water depth (Jerolmack, 2009; Wang et al., 2019). Digitate shallow-water deltas form with basin water depths of a few meters and basin slopes of less than 0.1° (Table 1). When wave and tide processes are weak, the upstream conditions are the primary cause of the geomorphic diversity of digitate shallow-water deltas. The diverse bar finger morphologies in Poyang Lake support the above perspective (Fig. 1G–I). However, it needs to be further studied how the upstream conditions influence digitate shallow-water delta morphology quantitatively.

In this study, we explored digitate shallow-water delta morphology and addressed the following three questions: 1) How can digitate shallow-water delta morphology be quantified? 2) How do the upstream conditions influence digitate shallow-water delta morphology? 3) Can digitate shallow-water delta morphology be quantitatively predicted based on the upstream conditions? We combined numerical modeling (Delft3D) with a dataset of modern deposits to quantify digitate shallow-water delta morphology and established empirical equations to quantify the effects of the upstream conditions. Section 2 overviews the theoretical basis of delta morphology and its controlling factors; Sections 3 describes the principles, assumptions, and parameters of Delft3D simulations; Section 4 defines morphologic metrics; Sections 5 quantifies metrics and their relations with upstream conditions in simulations; Section 6 presents the examination of modern deposits and application to an ancient reservoir, and discuss the connection between upstream conditions and delta morphology.

2. Background

To evaluate the effects of the upstream fluvial conditions, we need to

Fig. 1. Landsat images of typical digitate deltas. (A) Modern Mississippi River Delta (Gulf of Mexico, US); (B) Guadalupe Delta (San Antonio Bay, US); (C) Yellow River Delta (Bohai Sea, China); (D) Wulan Delta (Java Sea, Indonesia); (E) Birch River Delta (Lake Claire, Canada); (F) modern digitate shallow-water deltas in the Poyang Lake (China) and locations of Fig. 1G–I; (G) Longquan River Delta; (H) DSD1–DSD3; (I) DSD4 and DSD5. The blue curves indicate the distributary channels. The first two deltas are modern digitate deep-water deltas and the others are modern digitate shallow-water deltas. DSD: digitate shallow-water delta. (For interpretation of the references to colour in this figure legend, the reader is referred to the Web version of this article.)

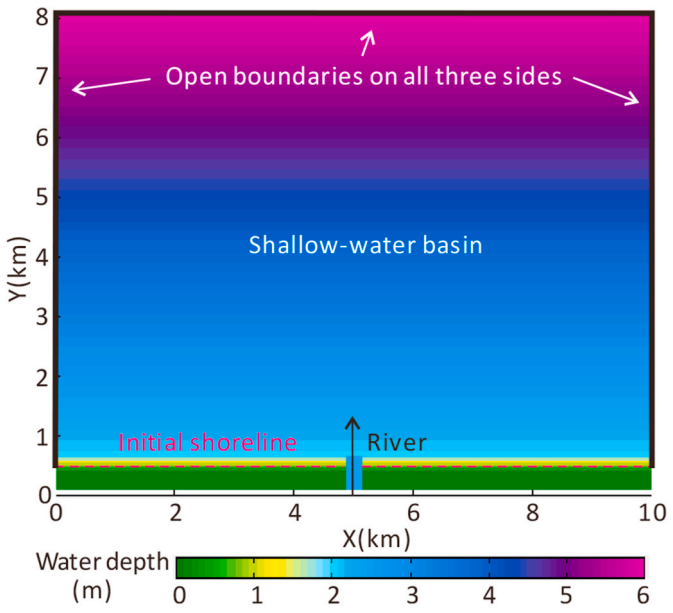

Fig. 2. Map view of the numerical Delft3D model setup. The grid cells have dimensions of 25 m × 25 m. The black arrow indicates the flow direction of the river. The black solid lines are open boundaries.

quantify digitate shallow-water delta morphology. Scholars have focused on two types of metrics to quantify delta morphology: one type pertains to external shapes, such as the delta width and delta length; Caldwell and Edmonds (2014), shoreline rugosity (Wolinsky et al., 2010; Caldwell and Edmonds, 2014; Burpee et al., 2015), and shoreline protrusion angle (Nienhuis et al., 2020); whereas the other type relates to the distributary channel network, such as the number of distributary channels (Syvitski and Saito, 2007; Edmonds and Slingerland, 2010; Burpee et al., 2015), bifurcation angle (Wright, 1977; Edmonds and Slingerland, 2007), bifurcation length and width (Olairu and Bhattacharya, 2006; Edmonds and Slingerland, 2007), and fractal dimension (Edmonds et al., 2011). The above metrics have been adopted to characterize the morphology of lobate deltas that encompass sheet distributary-mouth bars and complicated distributary channel networks. In contrast, digitate deltas are characterized by separate, sinuous bar fingers with rugose shorelines, few bifurcations, and low fractal dimensions, so the values of the above metrics measured for different digitate shallow-water deltas mostly exhibit low variability, except those of the delta length and number of distributary channels. Therefore, we adopted delta length (represent the farthest offshore-progradation distance of bar fingers) and the number of bar fingers (equal to number of distributary channels) to quantify the external shape of the digitate shallow-water delta. In addition, for digitate shallow-water delta, it is critical to quantify bar finger morphology, which is similar to sinuous river channel morphology. We also adopted sinuosity and width to quantify bar finger morphology, because these two metrics are widely applied to quantify sinuous river channel morphology (e.g. Schumm and Khan, 1972; Kleinhans and van den Berg, 2011; Constantine et al., 2014). In summary, we adopted four metrics: the bar finger sinuosity, bar finger width, delta length, and the number of bar fingers. To compare different scales of digitate deltas, the nondimensional bar finger width and delta length were adopted, which were defined as the ratio of the bar finger width and distributary channel width, and the ratio of delta length and distributary channel width, respectively. Descriptions of metrics see in Section 4.

Mouth bar width, delta length, and sinuosity and number of distributary channels in river-dominated deltas have been considered to be functions of some of the upstream fluvial variables, including sediment cohesion, sand proportion, sediment concentration, water discharge. Low sand proportion and high cohesion promote levee aggradation and stability, and consequently produce few elongated and sinuous distributary channels; in contrast, coarse-grained and low-cohesive sediments promote bifurcations, resulting in numerous terminal distributary channels (Orton and Reading, 1993; Edmonds and Slingerland, 2010; Geleynse et al., 2011; Caldwell and Edmonds, 2014; Burpee et al., 2015). High water discharge increases the number of distributary channels and deltaic land area (Syvitski and Saito, 2007) and increases delta length (Galloway, 1975; Olariu et al., 2012). In addition, a high sediment concentration can widen the mouth bar (Edmonds and Slingerland, 2007). Similarly, the four metrics we proposed for the digitate shallow-water delta are also functions of the upstream fluvial variables. Caldwell and Edmonds (2014) found that some morphologic metrics can achieve a dynamic equilibrium through time, whereas others cannot. Therefore, we must consider metric changes through sediment supply.

The downstream conditions also control delta morphology via the basinal water depth (e.g., Jerolmack, 2009; Carlson et al., 2018; Wang et al., 2019), and wave/tide processes (e.g., Bhattacharya and Giosan, 2003; Dalrymple and Choi, 2007; Jerolmack and Swenson, 2007; Plink-Bjorklund, 2012; Nardin et al., 2013). In shallow-water basins (mostly lakes), the water depth is only a few meters, and the tide process is negligible. Wind waves in shallow-water lakes exhibit small amplitudes, high frequencies, and short wavelengths (e.g., Allan and Kirk, 2000; Hofmann et al., 2008), and wave-induced mass transport is negligible (Ji and Jin, 2014). Wind waves in shallow waters can substantially increase sediment resuspension from the lake bed, which may influence the delta (Aalderink et al., 1985; Chung et al., 2009; Kelderman et al., 2012). However, there is no evidence that sediment resuspension significantly affects river-dominated delta morphology. If considering weak wave and tidal energies and similar shallow-water

Table 1
Depositional conditions of modern digitate shallow-water deltas based on Morton and Donaldson (1978), Molnar (1994), Yang and Wang (1995), Wang and Liang (2000), Syvitski and Saito (2007), Edmonds and Slingerland (2010), Milliman and Farnsworth (2013), Marfai et al. (2016), Timoney and Lee (2016), and Huang et al. (2017). Fig. 1 shows the locations of these modern deltas. DSD: digitate shallow-water delta.

Modern digitate shallow-water deltas	Sediment cohesion (N/m^2)	Sand proportion	Water discharge (m^3/s)	Sediment concentration (kg/m^3)	Sediment supply[a]($\times 10^7$ t)	Basin water depth (m)	Distributary channel depth(m)	Tide/ wave
Guadalupe Delta	1.5	0.2	93	0.3	4.24	2	5	weak
Wulan Delta	–	0.3	676	–	3.18	3	3	weak
Birch River Delta	1.5	0.3	1.33	0.3	4.77	1.5	2.3	weak
Longquan River Delta	2	0.1	50	0.1	5.30	2	2.5	weak
DSD1	1.5	0.2	280	0.1	3.45	2	2.5	weak
DSD2	1.5	0.2	200	0.1	3.45	2	2.5	weak
DSD3	2	0.25	200	0.1	4.24	2	2.5	weak
DSD4	1.5	0.25	200	0.1	9.54	2	2.5	weak
DSD5	1.5	0.3	700	0.1	11.66	2	2.5	weak

[a] The sediment supply was estimated using the 0.9 times of sediment mass (0.9 × area × average thickness × density) because most of the sediments were trapped by fluvial-dominated delta with a sediment trapping efficiency of ~0.9 (Wolinsky et al., 2010).

environments, the upstream fluvial conditions are critical factors for shallow-water digitate delta morphology, which is our focus in this study.

Multiple, narrow, and sinuous bar fingers and their distributary channels in shallow-water digitate delta reservoir is difficult to be finely described based on well data as well as seismic data. Predictive metrics can help to characterize inter-well distribution of bar fingers. Bar finger width (hundreds of meters) can be estimated by well data and seismic data, but distributary channel width (tens of meters) in the bar finger cannot. Predictive nondimensional bar finger width can be used to estimate distributary channel width. Predictive bar finger sinuosity and the number of bar fingers and delta length assist to describe bar finger boundaries. To predict metrics, we need to estimate depositional conditions during ancient shallow-water digitate delta growth. Burpee et al. (2015) attempted to determine the paleomorphology of the Last Chance Delta based on estimation of depositional conditions: wave and tidal energies were weak estimated by the development of related sedimentary structures; basinal water depth was 10–30 m approached to foreset thickness; water discharge was 1250 m^3/s estimated by estimating flow velocities and channel cross-sectional areas; the sand proportion was 81% calculated by vertical lithological characteristics; Sediment cohesion was high that qualitatively evaluated by climate and thickness of coal deposits. Finally, they proposed that the Last Chance Delta was intermediate between a fan and a bird-foot delta. They give us some insights and supports to predict ancient shallow-water digitate delta morphology by estimating depositional conditions.

3. Numerical simulation method

Numerical simulations were performed in this study to quantify the effects of the upstream conditions on digitate shallow-water delta morphology. Delft3D (Version 4.01.01) is effective software for shallow-water delta simulations (e.g., Edmonds and Slingerland, 2010; Geleynse et al., 2011; Caldwell and Edmonds, 2014; Burpee et al., 2015).

3.1. Description of the Delft3D model

Delft3D is a physics-based morphodynamic model based on numerical fluid flow and sediment transport models (WL|Delft Hydraulics, 2003). The flow is computed by solving the depth-integrated, Reynolds-averaged Navier–Stokes equations for incompressible and free surface flow. The morphological changes are updated using the Exner equation for sediment mass conservation.

From several transport formulas, the formulation of Van Rijn (1993) was chosen in this study. This formulation can distinguish between suspended and bedload transport during hydrodynamic computation. Fine sediments (diameter $\leq$64 μm) were considered to be cohesive sediments transported in suspension, whereas coarse sediments (diameter >64 μm) were considered to be non-cohesive sediments transported in suspension and bed loads (Grasmeijer et al., 2011; Chaichitehrani et al., 2019). The suspended-load transport was estimated using the 3D depth-averaged advection-diffusion equation, and the bedload transport was solved by utilizing a formula from Van Rijn (1993).

The direction of bedload transport was adjusted according to the bed-slope effects (Bagnold, 1966; Ikeda, 1982). The Delft3D model encompasses several sediment transport predictors for bed-slope effect estimation. Here, we chose the predictor of Van Rijn (1993), which can distinguish bed loads from suspended loads and promote more realistic sediment transport and morphological adaptation (Baar et al., 2019). However, this predictor may lead to severe and unrealistic channel incisions (Van der Wegen and Roelvink, 2012; Schuurman et al., 2013; Baar et al., 2019). Parameterizations of transverse slopes reflect the uncertainty of the non-linearity of sediment transport and the negative feedback on run-away deepening. Increasing the transverse bed slope parameters may counteract unrealistic incisions and produce realistic bar and channel patterns (Ikeda, 1982; Van der Wegen, 2009). Two parameterizations of transverse slopes by Bagnold (1966) and Ikeda (1982) are frequently used in the Delft3D model to calculate the downslope sediment transport vector differently (Dissanayake et al., 2009). The slope parameterization of Ikeda (1982) is more suitable for the predictor of Van Rijn (1993) because of its greater ability to counteract unrealistic incisions (Baar et al., 2019).

3.2. Model setup

Regarding the Delft3D model setup, we referred to modern digitate shallow-water deltas supplied by the Ganjiang River in Poyang Lake, China (Fig. 1G–I). Poyang Lake is the largest freshwater lake in China and was formed in approximately A.D. 400 (Fig. 1F). Its length is ~110 km north-south, and its width is 50–70 km east-west (Xu et al., 2001), covering an area of ~4125 km^2 (Shankman et al., 2006). The lake bed has a gentle basin slope of less than 0.1° and an average water depth of 8.4 m, with weak wave and tide processes (Min et al., 1995). From the hydrologic and core data, we acquired the upstream fluvial conditions of the digitate shallow-water deltas: the sand proportion is ~0.2; sediment cohesion (quantified by the critical shear stress for cohesive sediment erosion) is ~2 N/m^2, sediment concentration is ~0.1 kg/m^3, mean annual water discharge is ~400 m^3/s, and sediment supply is 3–12 × 10^7 t. In bar fingers, mouth bars, and distributary channels mostly consist of fine sands (D_{50} ~ 150 μm), and the levees consist of silt-mud sands (D_{50} = 80–30 μm). The marsh and bay deposits have muddy compositions (D_{50} < 30 μm).

Modern digitate shallow-water deltas in the Poyang Lake were used to determine the scale, morphometrics, and depositional conditions of the simulation S0. The model domain was 10 km × 8 km with 250 × 200 grid cells (Fig. 2). The initial basin slope was ~0.046°, and the water level was constant at 0 m. The initial river, 500 m long, 280 m wide, and 2.5 m deep, was located at the center of the model in the south (Fig. 2). The sediment supply was steady, and the open basin was unaffected by wave and tide processes. The sediment composition may influence the delta architecture (Van der Vegt et al., 2020). Based on sediment samples, we used a sediment mixture that contained sediments with grain diameters of 300, 150, 80, 32, 13, and 7.5 μm and had a roughly normal grain size distribution. Upstream fluvial conditions in the simulation S0 were that: the sand proportion was 0.25, sediment cohesion was 2 N/m^2, water discharge was 1200 m^3/s, and sediment concentration was 0.1 kg/m^3. The four additional groups of simulations were designed by individually changing the sediment cohesion (1–3.5 N/m^2, simulations S0–S5), sand proportion (0–1, simulations S0 and S6–S10), water discharge (200–1600 m^3/s, simulations S0 and S11–S15), and sediment concentration (0.05–0.3 kg/m^3, simulations S0 and S16–S20) (Table 2). The same sediment supply (4.84 × 10^7 t) was utilized in all simulations, except that simulation S11 only accepted a sediment supply of 3.23 × 10^7 t because of distributary channels outside the model domain. The sediment supply approached that in modern digitate shallow-water deltas (Table 1). The morphological scale factor was 175, which provided an increased rate of morphological change (Burpee et al., 2015). Transverse slope parameterizations 1.5–100 were tested, and a default value of 1.5 was chosen because the parameterization values had little effect on the morphological metrics of the digitate shallow-water deltas, including channel over-deepening. The cell size (10–40 m) and morphological scale factor (1–175) were also tested, which had little effect on the morphological metrics. Table 3 lists the other parameters.

In some simulations, aiming to shorten the simulation time, the water discharge was made higher than those of the digitated shallow-water deltas in Poyang Lake and approached the mean annual water discharge of the Ganjiang River (~1200 m^3/s). In addition, discharge and water-level variation (including flood events) were not considered, which may have increased the frequency of avulsions (Stouthamer and Berendsen, 2007; Edmonds et al., 2010; Harris et al., 2020; Wang et al., 2020). We observed that some digitate shallow-water deltas with few avulsions also formed in Poyang Lake (Fig. 1H). Although vegetation

Table 2
Detailed design of simulations.

ID	Sediment cohesion (N/m^2)	Sand proportion[a]	Water discharge (m^3/s)	Sediment concentration (kg/m^3)	Simulated hours	Sediment supply (× 10^7 t)
S0	2.0	2:8	1200	0.1	640	4.84
S1	1.0	2:8	1200	0.1	640	4.84
S2	1.5	2:8	1200	0.1	640	4.84
S3	2.5	2:8	1200	0.1	640	4.84
S4	3.0	2:8	1200	0.1	640	4.84
S5	3.5	2:8	1200	0.1	640	4.84
S6	2.0	0	1200	0.1	640	4.84
S7	2.0	1:9	1200	0.1	640	4.84
S8	2.0	3:7	1200	0.1	640	4.84
S9	2.0	4:6	1200	0.1	640	4.84
S10	2.0	1:1	1200	0.1	640	4.84
S11	2.0	2:8	200	0.1	2560	3.23
S12	2.0	2:8	600	0.1	1280	4.84
S13	2.0	2:8	800	0.1	960	4.84
S14	2.0	2:8	1000	0.1	768	4.84
S15	2.0	2:8	1600	0.1	480	4.84
S16	2.0	2:8	1200	0.05	1280	4.84
S17	2.0	2:8	1200	0.15	426	4.84
S18	2.0	2:8	1200	0.2	320	4.84
S19	2.0	2:8	1200	0.25	256	4.84
S20	2.0	2:8	1200	0.3	213	4.84

[a] Proportions of sediment compositions (300, 150, 80, 32, 13, and 7.5 μm): 0%, 0%, 0%, 20%, 60%, and 20% (sand proportion is 0); 0%, 0%, 10%, 50%, 30%, and 10% (sand proportion is 1:9); 0%, 5%, 15%, 40%, 30%, and 10% (sand proportion is 2:8); 5%, 5%, 20%, 40%, 20%, and 10% (sand proportion is 3:7); 5%, 10%, 25%, 35%, 20%, and 5% (sand proportion is 4:6); 5%, 15%, 30%, 30%, 15%, and 5% (sand proportions is 1:1).

Table 3
Parameters in simulation S0.

Simulated parameter	Value	Unit
Water surface elevation of open boundaries	0	m
Initial sediment layer thickness at bed	10	m
Time step	0.2	min
Morphological scale factor	175	
Chézy value for hydrodynamic roughness	45	m^2/s
Background horizontal eddy viscosity and diffusivity	0.001	m^2/s
Spin-up interval before morphological updating begins	1440	min
Factor for the erosion of adjacent dry cells	0.25	–
Cohesive sediment critical shear stress for deposition	1000	N/m^2

was not simulated directly, it was partly considered by increasing the cohesion of the muddy composition.

Fig. 3 illustrates the morphology of the simulated digitate shallow-water deltas. We defined deltaic land cells as having water depths less than 0.5 m (Dark green area in Figs. 3 and 4A) and identified the active channel skeletons as having water depths greater than 1 m and depth-averaged velocities greater than 1.3 m/s. The combined active and abandoned channel skeletons were acquired by overlapping the time-series active channel skeleton (A calculation of simulation S0 is shown in Fig. 4B). Then, we could calculate the time-series sinuosity, width, number of bar fingers, and delta length (see below).

4. Descriptions of metrics

1) The number of bar fingers was the same as the number of distributary channels including all active and abandoned distributary channels in a digitate shallow-water delta (Fig. 4B). We counted the bar fingers longer than three times the width of the river mouth to avoid counting many insignificant short bar fingers.
2) The bar finger sinuosity was defined as the ratio of the physical length (centerline length) to the linear distance between the end-points of the bar finger (Fig. 4A). The average bar finger sinuosity was adopted to represent the average sinuosity of the bar fingers in a digitate shallow-water delta (Fig. 4).
3) The width of the bar finger (or distributary channel) in a digitate shallow-water delta was calculated as the ratio between the area and length of the bar finger (or distributary channel). The average width of the bar finger was adopted to represent the average width of the bar fingers in a digitate shallow-water delta, which was calculated as the ratio between the total delta area and total bar finger length. Similarly, the average width of the distributary channel was calculated as the ratio between the total distributary channel area and total distributary channel length. Wide rivers commonly create wide distributary channels and bar fingers (Fig. 1). To compare different scales of digitate deltas, the nondimensional average width of bar fingers was defined as the ratio between the average bar finger width and average distributary channel width. If considering that total bar finger length approached the total distributary channel length, the nondimensional average bar finger width was defined as the ratio between the total delta area and total distributary channel area (Fig. 4B and C).
4) The delta length was defined as the maximum beach-perpendicular distance in a delta (Caldwell and Edmonds, 2014, Fig. 4A) and represented the farthest offshore-progradation distance between bar fingers. The nondimensional delta length was defined as the ratio between the delta length and average distributary channel width, so as to compare different scales of digitate deltas.

5. Results

5.1. Quantified effects of upstream conditions on simulated digitate shallow-water delta morphology

We quantified the relationships between the morphologic metrics and upstream conditions based on the simulation results (Fig. 4) and considered how the metric have changed as the sediment supply increased. Due to the value of sediment supply being large, the nondimensional sediment supply was defined as the ratio between the sediment supply and 4.84 × 10^7 t so that the value of the nondimensional sediment supply ranged from 0 to 1 for all simulations and ranged from 0 to 10 for natural deltas.

5.1.1. Bar finger sinuosity

Bar fingers within digitate shallow-water deltas display a wide range of sinuosities, but the average sinuosities exhibit close relationships with the upstream conditions after 100% nondimensional sediment supply (Fig. 5). The average sinuosities exhibit good linear relationships with

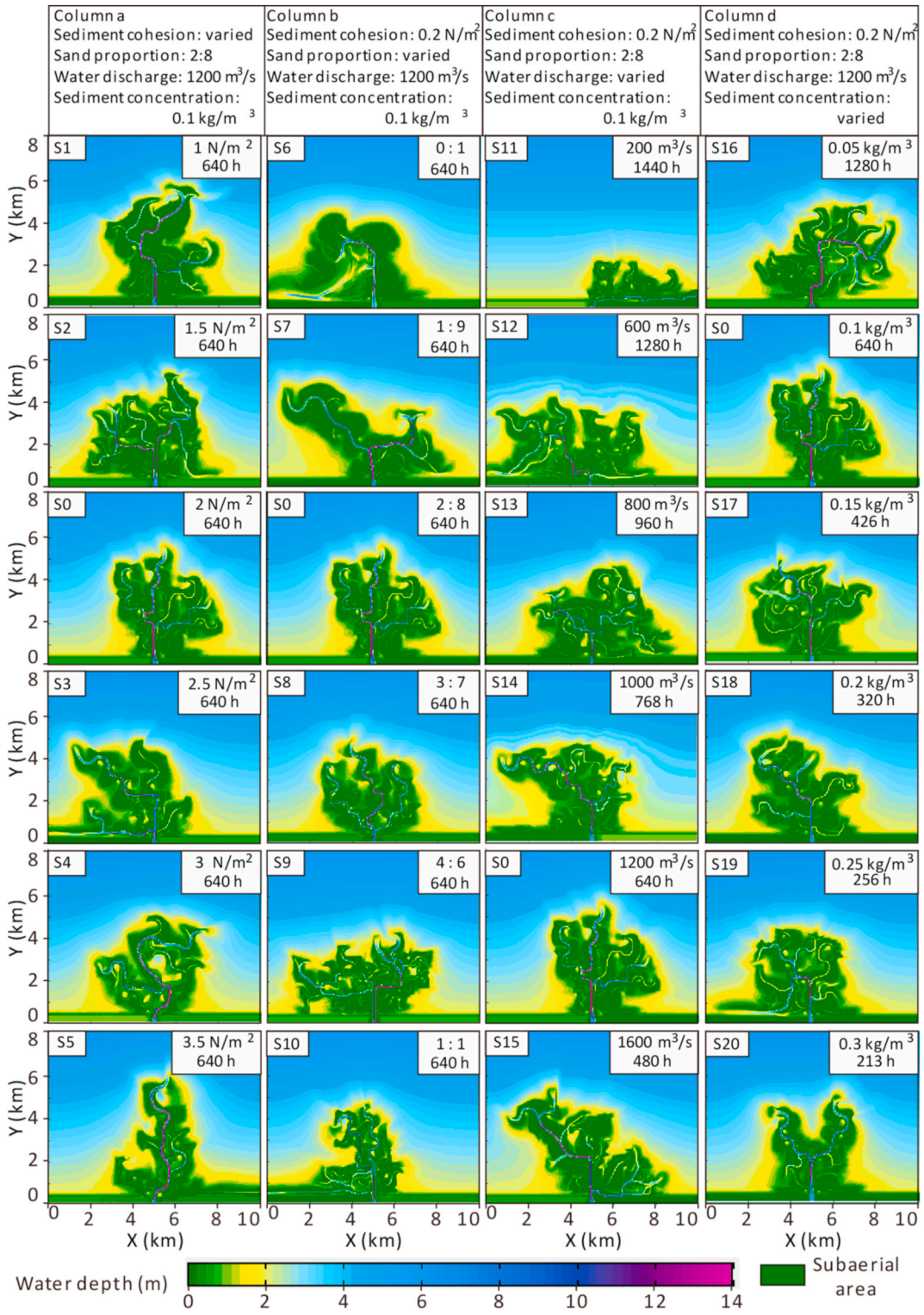

Fig. 3. Map views of simulated digitate shallow-water deltas (S0–S20) after accepting 4.84×10^7 t of sediment supply, except in the case of simulation S11, in which 3.23×10^7 t of sediment supply was accepted.

the sediment cohesion ($R^2 = 0.83$) and sediment concentration ($R^2 = 0.86$) and inverse linear relationships with the sand proportion ($R^2 = 0.81$) and water discharge ($R^2 = 0.87$) (Fig. 5). With the same sediment supply, a high sediment cohesion and concentration, and low sand proportion and water discharge promote the formation of high-sinuosity bar fingers (Figs. 5 and 6).

The sinuosities of the bar fingers increase as the sediment supply increases, especially when nondimensional sediment supply is less than 50% (Fig. 6). Although the average sinuosities of the bar fingers exhibit certain logarithmic increases as the sediment supply increases (some of the logarithmic relations are shown in Fig. 6), they generally increase less with some fluctuations after 50% nondimensional sediment supply, except in the cases of the digitate shallow-water deltas with low sand proportions (0 and 0.11), which exhibit stable average sinuosities until

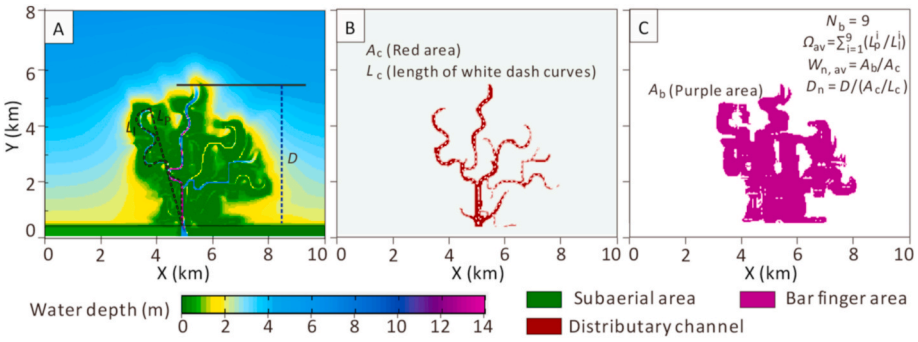

Fig. 4. Map views of simulation S0 (A) and its distributary channels (B), its bar finger area (C). N_b: number of bar fingers; Ω_{av}: average sinuosity of bar fingers; L_p: physical length (centerline length) of the bar finger; L_l: linear distance of the bar finger; $W_{n,av}$: nondimensional average width of bar fingers; A_b: total area of bar fingers; A_c: total area of distributary channels; D_n: nondimensional delta length; D: delta length; L_c: total length of distributary channels.

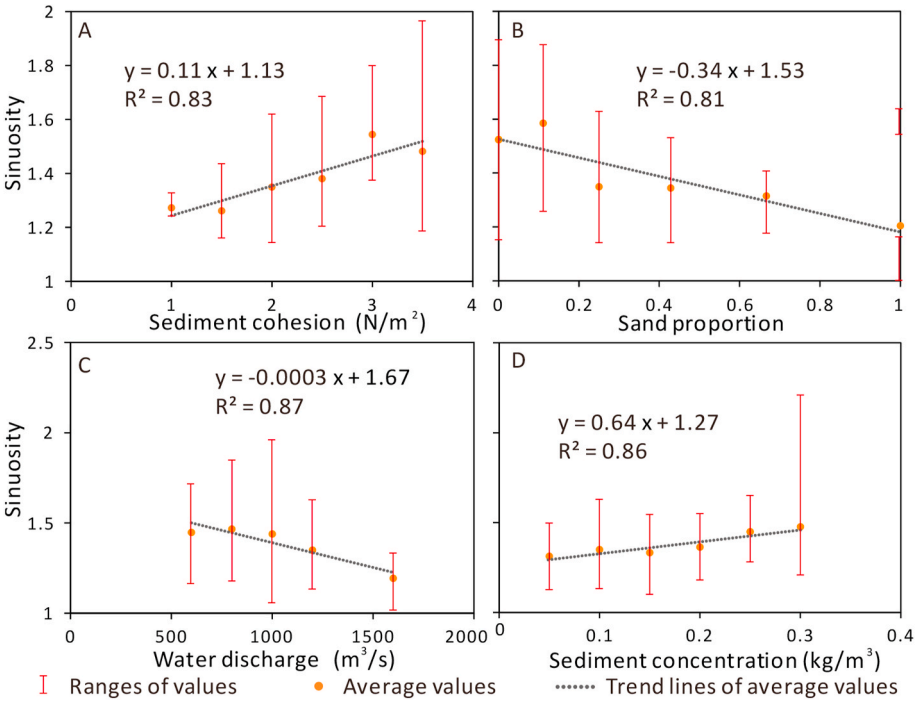

Fig. 5. Relationships between sinuosity and (A) sediment cohesion, (B) sediment proportion, (C) water discharge, and (D) sediment concentration after 4.84×10^7 t of sediment supply. The sinuosity in simulation S11 was estimated based on the trend when the sediment supply is less than 3.23×10^7 t The average sinuosity exhibits linear relationships with the sediment cohesion and sediment concentration and inverse linear relationships with the sand proportion and water discharge.

70% nondimensional sediment supply (Fig. 6B). We adopted Pearson, Kendall, and Spearman correlation coefficients (with ranges from −1 to 1) to assess the statistical dependence between the average sinuosity and sediment supply. High absolute values indicate a close correlation between the considered variables. The average sinuosity exhibits a certain relationship with the sediment supply, but it has almost no correlation with the sediment supply when the nondimensional sediment supply is greater than 50% (Table 4). The modern deposits and simulated results show that bar fingers in a digitate shallow-water delta mostly have similar sinuosities (Figs. 1 and 4). When the nondimensional sediment supply is less than 50%, the number of bar fingers is mostly ≤5; at this point, one low sinuosity finger can much induce decreased average sinuosity of the bar fingers. When the nondimensional sediment supply is greater than 50%, the number of bar fingers is mostly more than 5; at this point, the sinuosity of bar fingers approaches an equilibrium and is independent of sediment supply. A reference nondimensional sediment supply value of 50% causes the average sinuosity to approach equilibrium.

According to the above results (Figs. 5 and 6), the average sinuosity of the bar fingers (Ω_{av}) has the following relationship with upstream conditions:

$$\Omega_{av} = (a\tau - bR_S - cQ + dC + e)\ln(10S_n) + f, \quad (1)$$

where τ is the sediment cohesion, R_S is the sand proportion, Q is the water discharge, C is the sediment concentration, and S_n is the nondimensional sediment supply; a–f are positive constants.

Based on multivariate regression, we get solutions of the a–f, and then Ω_{av} can be quantified as a function of the upstream conditions:

$$\Omega_{av} = (0.060\tau - 0.093R_S - 0.00006Q + 0.15C + 0.20)\ln(10S_n) + 0.99, \quad (2)$$

R^2 is 0.67. The low sinuosity of the bar finger has a low Ω_{av} value, and the straight bar finger has a minimum Ω_{av} value of 1. Hence, if the predicted Ω_{av} value < 1, Ω_{av} should be 1.

If the nondimensional sediment supply is more than 50%, Ω_{av} is weakly related to the sediment supply, so equation (2) can be simplified as

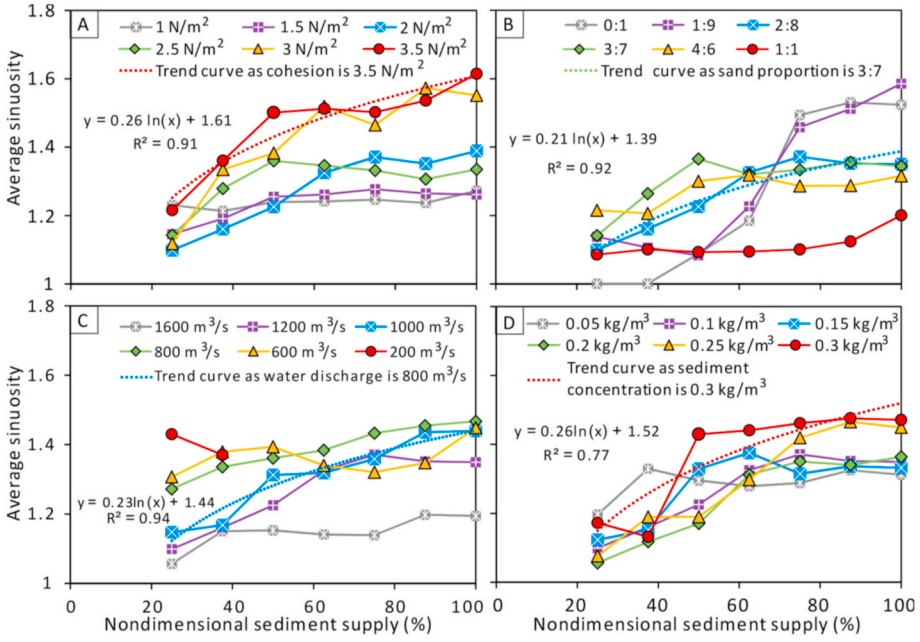

Fig. 6. Relationship between average sinuosity and nondimensional sediment supply with different (A) sediment cohesions, (B) sand proportions, (C) water discharges, and (D) sediment concentrations. The average sinuosity initially increases when the sediment supply increases, whereas it changes little with some fluctuations after the nondimensional sediment supply exceeds 50%. In some simulations, the average sinuosity exhibits a positive logarithmic relationship with the nondimensional sediment supply. For the same sediment supply, high-sinuosity bar fingers tend to form with a high sediment cohesion and sediment concentration and low sand proportion and water discharge.

Table 4
Correlative analysis between average sinuosity and nondimensional sediment supply. A high absolute value of the correlative coefficient reflects a strong correlation between the average sinuosity and nondimensional sediment supply.

Correlative coefficient	Nondimensional sediment supply	
	>0%	>50%
Pearson correlative coefficient	0.303	0.113
Kendall correlative coefficient	0.396	0.158
Spearman correlative coefficient	0.528	0.203

$$\Omega_{av} = 0.14\tau - 0.25R_S - 0.00006Q + 0.45C + 1.20, \quad (3)$$

where R^2 is 0.62. If the predicted Ω_{av} value < 1, Ω_{av} should be 1.

5.1.2. Bar finger width

The average nondimensional width was adopted to quantify the width of the bar fingers in a digitate shallow-water delta. Its value generally varied within 10% as the sediment supply increases, especially after 30% nondimensional sediment supply (Fig. 7). Although it exhibits a logarithmic increase as the sediment supply increases ($R^2 > 0.9$) for digitate shallow-water deltas with low cohesion (1–2.5 N/m^2), it increases slowly after 30% nondimensional sediment supply. The low absolute values of Pearson, Kendall, and Spearman correlation coefficients indicate that the average nondimensional width is poorly related to the sediment supply, especially after 30% nondimensional

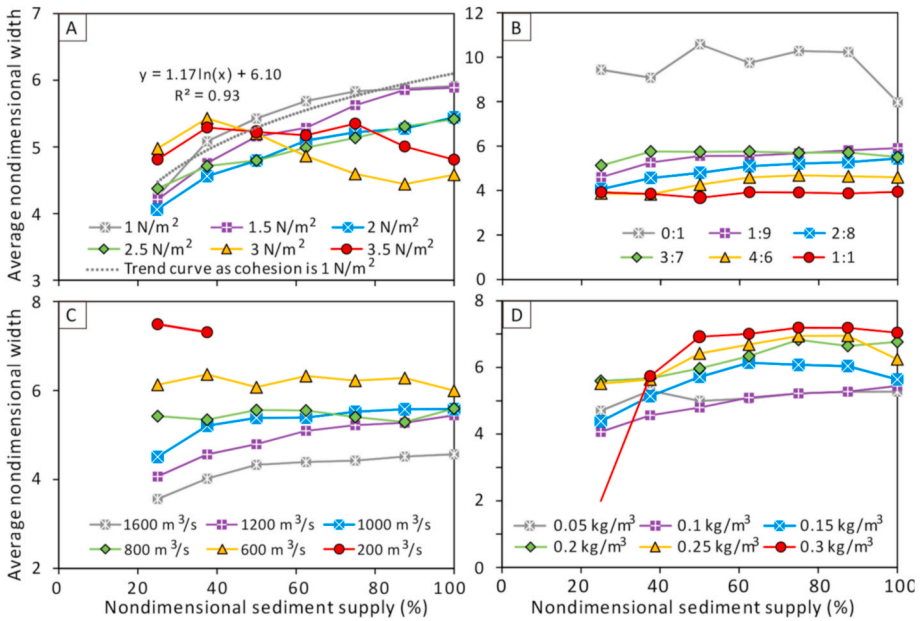

Fig. 7. Relationship between average nondimensional width and nondimensional sediment supply with different (A) sediment cohesions, (B) sand proportions, (C) water discharges, and (D) sediment concentrations. The average nondimensional width changes little when the sediment supply increases. Although the average nondimensional width logarithmically increases when the sediment supply increases in low-cohesion (1–2.5 N/m^2) digitate shallow-water deltas, the rate of increase is slow. For the same sediment supply, a low sediment cohesion, sand proportion, and water discharge and high sediment concentration promote the formation of wide bar fingers.

Table 5
Analysis of correlation between average nondimensional width and nondimensional sediment supply. A high absolute value of the correlation coefficient reflects a strong correlation between the average nondimensional width and nondimensional sediment supply.

Correlation coefficient	Nondimensional sediment supply	
	>0%	>50%
Pearson correlation coefficient	0.175	−0.031
Kendall correlation coefficient	0.187	0.017
Spearman correlation coefficient	0.256	0.018

sediment supply (Table 5). The modern deposits and simulated results also reveal that the bar finger width is similar at different sections, excluding the terminal section, and that the widths of different bar fingers in a digitate shallow-water delta are similar (Figs. 1 and 4). Therefore, the upstream conditions determine a consistent bar finger width in a digitate shallow-water delta, which is unaffected by increases in sediment supply.

With the same sediment supply, a low sediment cohesion, low sand proportion, low water discharge, and high sediment concentration promote the formation of wide bar fingers (Fig. 7). At 100% nondimensional sediment supply, the average nondimensional bar finger width ($W_{n,\ av}$) is inversely proportional to the sediment cohesion ($R^2 = 0.85$), sand proportion ($R^2 = 0.87$), and water discharge ($R^2 = 0.91$) and proportional to the sediment concentration ($R^2 = 0.82$) (Fig. 8).

According to the above results (Figs. 7 and 8), $W_{n,\ av}$ has the following relationship with upstream conditions:

$$W_{n,\ av} = \left(-h\tau + \ ie^{-11.43R_S} - \ jQ + \ kC + \ l\right)\ln(10S_n) + m, \quad (4)$$

where h–m are positive constants.

Based on multivariate regression, we get solutions of the h–m, and then $W_{n,\ av}$ can be quantified as follows:

$$W_{n,\ av} = \left(-0.15\tau + 2.50e^{-11.43R_S} - 0.001Q + 4.45C + 1.32\right)\ln(10S_n) + 4.48, \quad (5)$$

where $R^2 = 0.726$.

If the effect of sediment supply is ignored, equation (3) can be simplified as

$$W_{n,\ av} = -0.19\tau + 4.67e^{-13.69R_S} - 0.002Q + 7.29C + 6.82, \quad (6)$$

where $R^2 = 0.724$. Equation (5) exhibits a similar fitting correlation to equation (6). Therefore, $W_{n,\ av}$ is not related to the sediment supply. Equation (6) is a better choice to quantify the bar finger width.

5.1.3. Delta length

The delta length increases as the sediment supply increases (Fig. 9). The nondimensional delta length (D_n) positively scales with the nondimensional sediment supply in a good logarithmic relationship ($R^2 > 0.95$) (some logarithmic relations are shown in Fig. 9). This logarithmic relationship indicates that the offshore-progradation rate gradually slows down as the delta grows.

When the sediment supply is the same, the delta length increases proportionally to the water discharge, whereas it is less influenced by the other upstream conditions (Figs. 9 and 10). Referencing a condition of 100% nondimensional sediment supply, D_n has an evident power-law relationship with the water discharge ($R^2 = 0.82$). Thus, high water discharges can drive the digitate shallow-water delta to prograde far away from the shoreline.

According to the above results (Figs. 9 and 10), D_n has the following relationship with upstream conditions:

$$D_n = nQ^{0.26}\ln 10S_n, \quad (7)$$

where n is a positive constant.

Based on multivariate regression, we get the solution of the n, and then D_n can be expressed as

$$D_n = 8.84Q^{0.26}\ln 10S_n, \quad (8)$$

where R^2 is 0.75. When $Q = 0$ or $S_n = 0$, $D_n = 0$.

5.1.4. Number of bar fingers

The number of bar fingers (N_b) includes both the active and

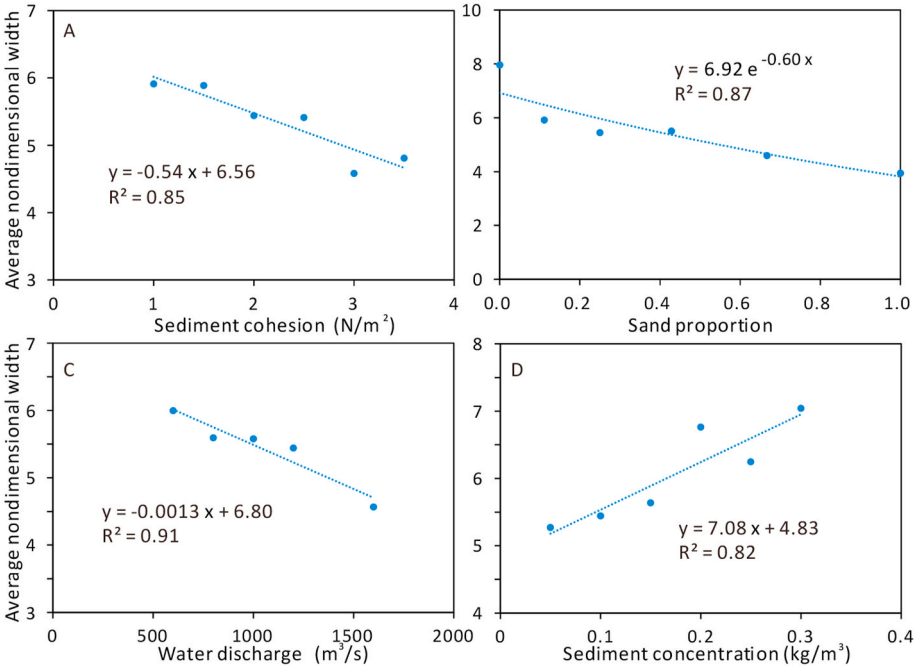

Fig. 8. Relationships between average nondimensional width of bar fingers and (A) sediment cohesion, (B) sediment proportion, (C) water discharge, and (D) sediment concentration after 4.84×10^7 t of sediment supply. The average nondimensional width exhibits negative linear relationships with the sediment cohesion ($R^2 = 0.85$), sand proportion ($R^2 = 0.87$), and water discharge ($R^2 = 0.91$) and a positive linear relationship with the sediment concentration ($R^2 = 0.82$).

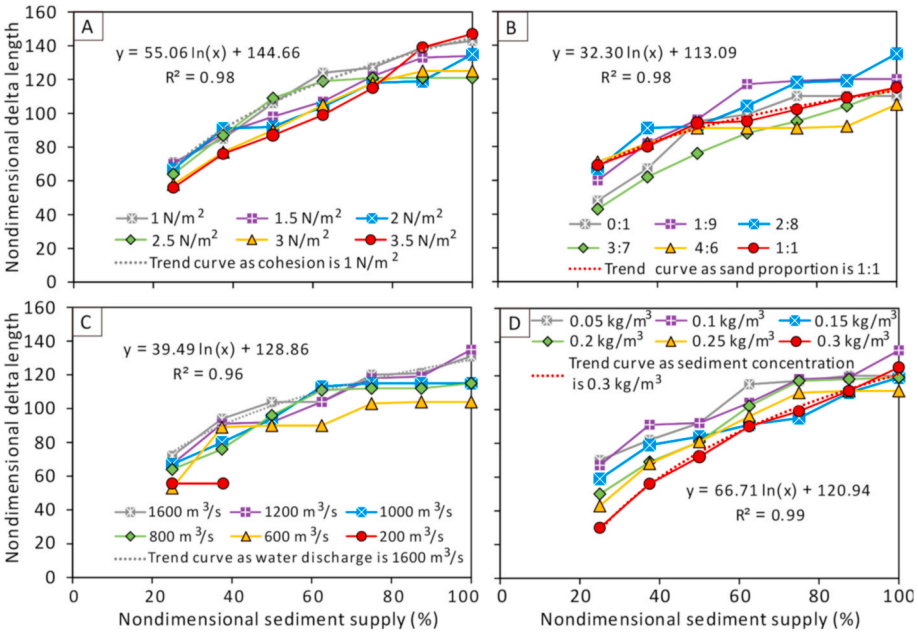

Fig. 9. Relationship between nondimensional delta length and nondimensional sediment with different (A) sediment cohesions, (B) sand proportions, (C) water discharges, and (D) sediment concentrations. Nondimensional delta length has a logarithmic relationship with nondimensional sediment supply ($R^2 > 0.95$). For the same sediment supply, high water discharge makes the bar fingers prograde basinward.

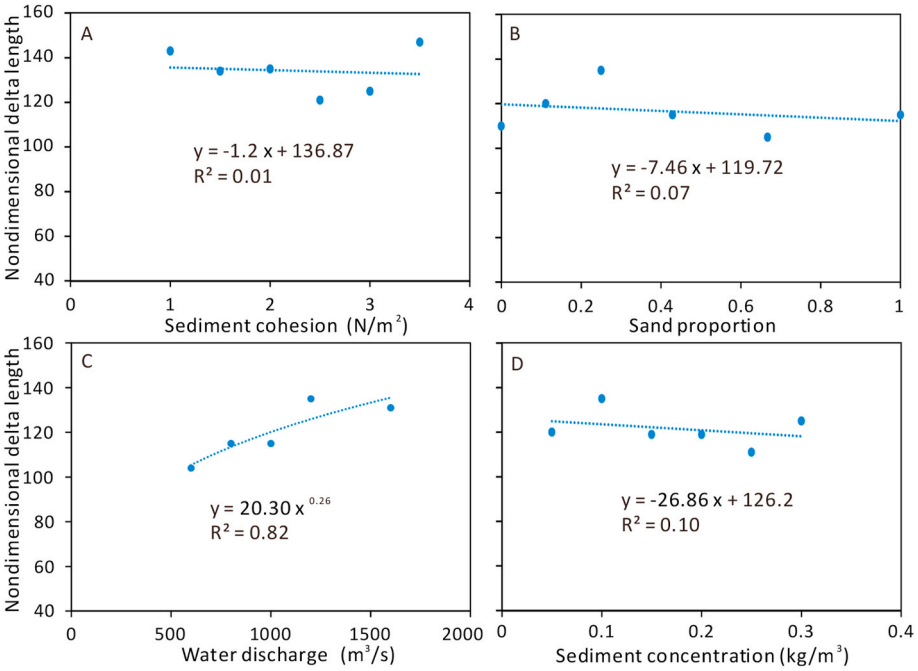

Fig. 10. Relationships between nondimensional delta length and (A) sediment cohesion, (B) sediment proportion, (C) water discharge, and (D) sediment concentration after 4.84×10^7 t of sediment supply. The nondimensional delta length is influenced by the water discharge alone and exhibits a positive power relationship with the water discharge ($R^2 = 0.82$).

abandoned bar fingers. It increases with increasing sediment supply and exhibits a positive linear relationship with the nondimensional sediment supply ($R^2 > 0.89$) (some linear relations are shown in Fig. 11).

For the same sediment supply, low sediment cohesion and high sand proportion promote the formation of more bar fingers, but the water discharge and sediment concentration have weak influences on N_b (Fig. 11). For example, when the nondimensional sediment supply is 100%, N_b is proportional to the sand proportion ($R^2 = 0.98$) and inversely proportional to the sediment cohesion ($R^2 = 0.69$) (Fig. 12).

According to the above results (Figs. 11 and 12), N_b has the following relationship with upstream conditions:

$$N_b = (-o\tau + pR_S + q)S_n + r, \quad (9)$$

Where o–r are positive constants.

The linear regression can be recast into an equation that quantifies N_b:

$$N_b = (-3.15\tau + 8.03R_S + 11.10)S_n + 1.84, \quad (10)$$

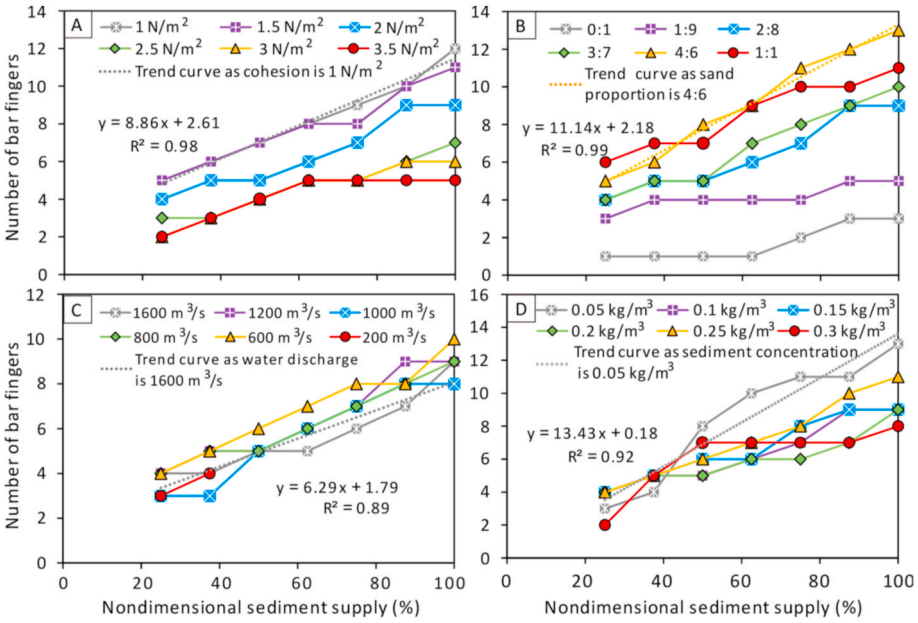

Fig. 11. Relationships between the number of bar fingers and nondimensional sediment supply under conditions of different sediment cohesions (A), sand proportions (B), water discharges (C), and sediment concentrations (D). The number of bar fingers and nondimensional sediment supply have a linear relationship ($R^2 > 0.89$). For the same sediment supply, low sediment cohesion and high sand proportion promote to form more bar fingers.

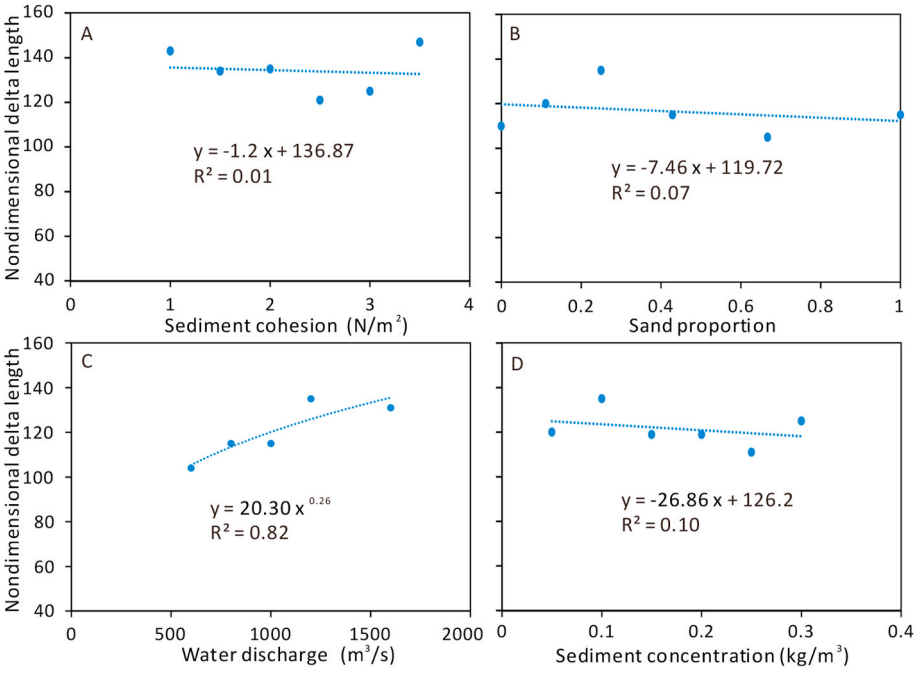

Fig. 12. Relationships between number of bar fingers and (A) sediment cohesion, (B) sediment proportion, (C) water discharge, and (D) sediment concentration after 4.84×10^7 t of sediment supply. The number of bar fingers exhibits good linear relationships with the sediment cohesion ($R^2 = 0.98$) and sand proportion ($R^2 = 0.69$) and weak linear relationships with the water discharge ($R^2 = 0.14$) and sediment concentration ($R^2 = 0.31$).

where N_b must be rounded to the nearest integer and R^2 is 0.75.

5.2. Correlation analysis of morphologic metrics

The simulated digitate shallow-water deltas exhibit various bar finger morphologies (Fig. 4) that are quantified by wide ranges of the morphological metrics: the average sinuosity is 1.0–1.61, average nondimensional bar finger width is 1.99–10.58, nondimensional delta length is 30–147, and the number of bar fingers is 1–13 (Fig. 13). In addition, the relationships among the metrics are poor ($R^2 < 0.3$).

Table 6 lists the values of these morphological metrics in nine modern digitate shallow-water deltas, which also show wide ranges: the average sinuosity ranges from 1.14 to 1.58, average nondimensional width ranges from 6.0 to 9.1, nondimensional delta length ranges from 63 to 163, and the number of bar fingers ranges from 3 to 21 (Table 6). Although the delta length and average width have a somewhat linear relationship ($R^2 = 0.41$), the other relationships among the metrics are poor (Fig. 14).

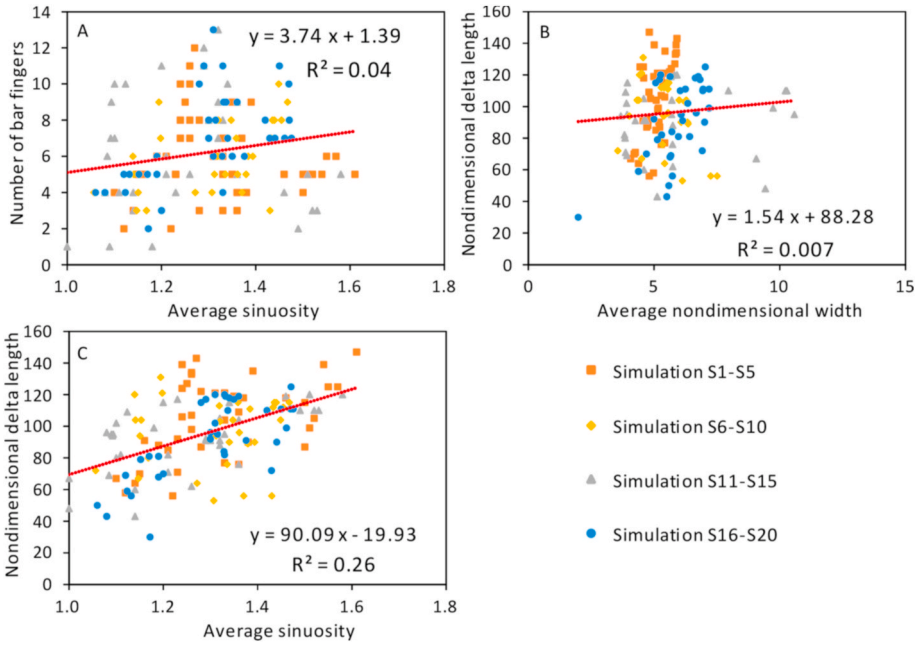

Fig. 13. Poor relationships between (A) number of bar fingers and average sinuosity, (B) nondimensional delta length and average nondimensional width, and (C) nondimensional delta length and average sinuosity based on simulation results. R^2 is less than 0.26 in each case.

Table 6
Measured morphological metrics of modern DSDs. Fig. 1 provides corresponding satellite images.

Modern digitate shallow-water deltas	Average sinuosity	Nondimensional delta length	Average nondimensional width	Number of bar fingers
Guadalupe Delta	1.19	63	7.0	8
Wulan Delta	1.14	63	8.8	3
Birch River Delta	1.28	48	9.1	8
Longquan River Delta	1.58	64	6.1	6
DSD1	1.38	71	7.0	6
DSD2	1.49	86	6.6	5
DSD3	1.31	107	6.7	6
DSD4	1.41	125	6.3	21
DSD5	1.31	163	6.0	20

6. Discussion

The wide-ranging morphologic metrics of a digitate shallow-water delta are poorly related to each other, making it difficult to predict one of the metrics using the others. Hence, empirical equations as functions of the upstream conditions are important for the morphologic prediction of digitate shallow-water deltas. However, the empirical equations obtained in this study were quantified based on the simulation results. The focus of this discussion is the applicability of the empirical equations based on modern deposits and links between upstream conditions and morphological metrics, and then apply empirical equations to predict the morphology of an ancient digitate shallow-water delta.

6.1. Examination of modern digitate shallow-water deltas

Based on the simulation results, we established five empirical equations [Equations ((2), (3), (6), (8) and (10)]. Nine modern digitate deltas that have developed in worldwide shallow-water lakes and bays (Fig. 1 and Table 1) were utilized to examine the applicability of these empirical equations. Table 1 summarizes the upstream conditions of the modern deposits. Then, we used the empirical equations to calculate the morphologic metrics, as shown in Table 7. The most of predicted values of average sinuosity of bar fingers, average nondimensional width of bar fingers, and nondimensional delta length well match the measured values with predictive errors <10% (Fig. 15A–C), whereas predicted values of the number of bar fingers limitedly match the measured values with predictive errors <50% (Fig. 15D). It indicates that the number of bar fingers may be significant influenced by downstream conditions (such as the ratio of distributary channel depth to basinal water depth). The average nondimensional width of the bar fingers in the Longquan River Delta and Guadalupe Delta and the average sinuosity of the bar fingers in the Guadalupe Delta are overestimated, may because the narrow lake or bay environments hinder lateral sediment transports (Fig. 1C and G). Most of the upstream conditions can be derived from hydrologic data or geological observations from modern deltas, especially those associated with human activities. Therefore, the empirical equations can predict the morphologies of digitate shallow-water deltas those form in open basins with weak wave and tide processes.

We attempted to use the empirical equations to predict the morphologies of modern digitate deep-water deltas, specifically, the modern Mississippi River Delta and Yellow River Delta. However, the predicted metrics deviate from the measured values (Fig. 15). The digitate deep-water deltas exhibit lower sinuosities, widths, lengths, and numbers of bar fingers than predicted. The measured numbers of bar fingers are much lower than the predicted values. Thus, the basin water depth decreases the sinuosity, width, length, and number of bar fingers. The downstream conditions (such as basin water depth, wave, and tide processes) are also important for delta formation and morphology (e.g., Caldwell et al., 2019; Nienhuis et al., 2020). Therefore, the empirical equations are not suitable for predicting digitate deep-water delta morphology. Linking the downstream conditions to digitate delta morphology could help improve the empirical equations.

6.2. How do upstream conditions affect digitate shallow-water delta morphology?

6.2.1. How do upstream conditions affect bar finger sinuosity

Xu et al. (2021) proposed that digitate shallow-water delta develops sinuous bar fingers because friction-dominated shallow-water delta

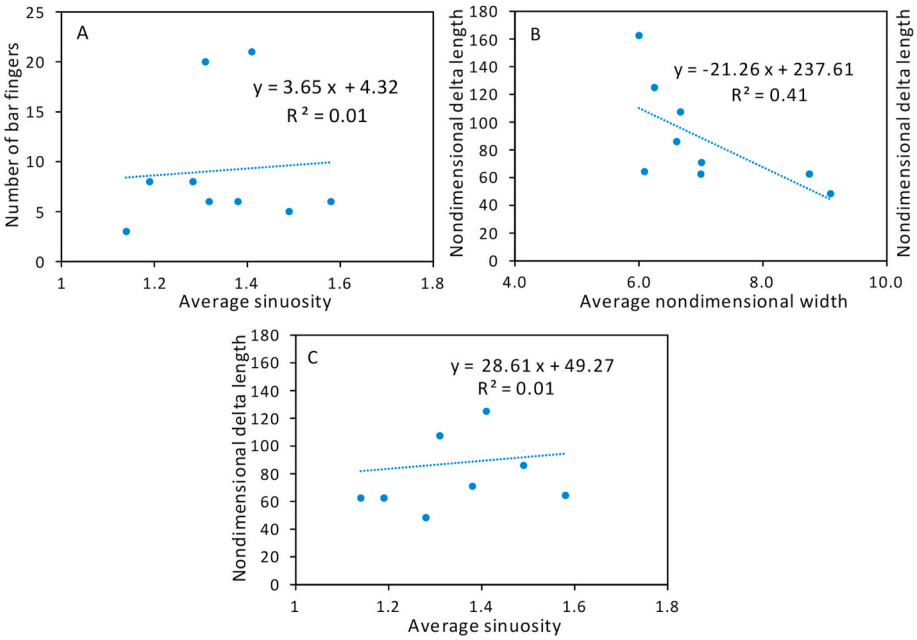

Fig. 14. Poor relationships between (A) number of bar fingers and average sinuosity, (B) nondimensional delta length and average nondimensional width, and (C) nondimensional delta length and average sinuosity based on modern digitate shallow-water deltas. The nondimensional delta length has a weak relationship with the average nondimensional width ($R^2 = 0.41$), whereas the other pairs exhibit no relationships.

Table 7
Predicted morphological metrics of modern DSDs based on empirical equations.

Modern digitate shallow-water deltas	Predicted metrics			
	Average sinuosity	Nondimensional delta length	Average nondimensional width	Number of bar fingers
Guadalupe Delta	1.49	62	8.84	10
Wulan Delta	–	91	–	–
Birch River Delta	1.47	22	8.80	12
Longquan River Delta	1.50	59	8.26	9
DSD1	1.39	75	7.01	8
DSD2	1.39	69	7.17	8
DSD3	1.45	76	6.92	9
DSD4	1.38	105	7.02	20
DSD5	1.34	154	5.94	24

effluents promote mouth bar deposition that then diverts flow around the mouth bar. They indicated that bar finger sinuosity is related to the dominance between bank strength and centrifugal force of water flow. High bank strength and low centrifugal force of water flow promote flow to extend around the mouth bar, resulting in the formation of more sinuous bar fingers. High sediment cohesion and low sand proportion increase bank strength (Hoyal and Sheets, 2009), in turn, increases bar finger sinuosity. High water discharge enhances the centrifugal force of water flow, leading to the formation of lowly sinuous bar fingers. Low sediment concentration improves erosion of water flow and then decreases bank strength, hence, it causes the formation of lowly sinuous bar fingers. Bar finger sinuosity is sediment supply independent since sediment supply is unrelated to the bank strength and centrifugal force of water flow.

6.2.2. How do upstream conditions affect bar finger width

Bar finger consists of mouth bar, distributary channel and levee deposits, and its width is approximate mouth bar width (Fisk, 1955; Xu et al., 2019, 2021), which is determined by outflow hydraulics. At the channel outlet, high lateral flow velocity and far lateral sediment transport distance increase mouth bar width. Simulation results illustrate that the lateral velocity of the water flow is high and the wide bar finger forms when sediment cohesion is low, sand proportion is low, water discharge is low, or sediment concentration is high (Fig. 16). Low sand proportion means high suspended loads, which can be far transported and promote the formation of wide bar fingers. High sediment cohesion reduces the ability of the system to re-erode deposited sediment, resulting in the formation of stable mouth bars and levees, and deep distributary channels (Edmonds and Slingerland, 2010); at this point, the water flow is highly concentrated on distributary channels and results in decreased bar finger width. High water discharge increases inertia outflow with a low spread angle (Wright, 1977), leading to create narrow bar fingers. High sediment concentration increases friction outflow with a large spread angle (Wright, 1977), resulting in the formation of wide bar fingers. The width of bar fingers is independent of sediment supply since sediment supply makes no difference to outflow hydraulics.

6.2.3. How do upstream conditions affect delta length

Delta length represents the farthest offshore-progradation distance of bar fingers, hence, high inertial force promotes large delta length. High water discharge provides high inertial force (Galloway, 1975; Olariu et al., 2012), illustrated by high flow velocity (Fig. 16), so that they can increase delta length. However, other upstream conditions have less influence on flow velocity. In addition, bar fingers need time and sediment supply to prograde offshore.

6.2.4. How do upstream conditions affect the number of bar fingers

The number of bar fingers is equal to the number of distributary channels, which decreases by enhancing distributary channel stability. Less cohesive deltas with high sand proportions have more laterally mobile channels with fewer avulsions and bifurcations due to more sediments with the higher cohesion deposited in channel banks makes banks more resistant to erosion (Hoyal and Sheets, 2009; Edmonds and Slingerland, 2010; Caldwell and Edmonds, 2014). As sediment supply increases, distributary channels continue to occur avulsions and bifurcations and form more distributary channels. Syvitski and Saito (2007) showed that the number of distributary channels covering a delta

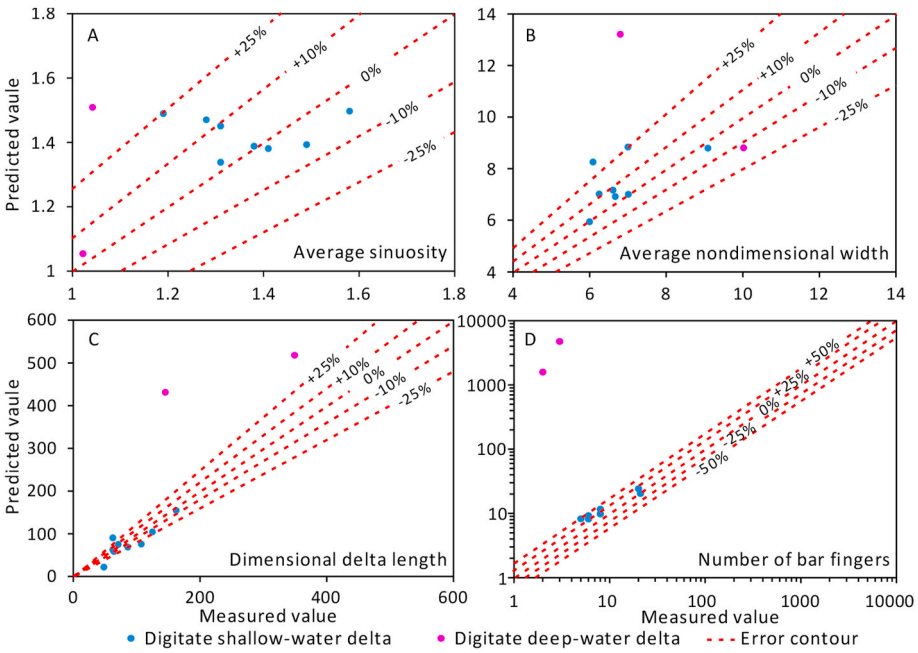

Fig. 15. Relationships between measured and predicted (A) average sinuosity, (B) average nondimensional width, (C) dimensional delta length, and (D) number of bar fingers of modern digitate shallow-water deltas.

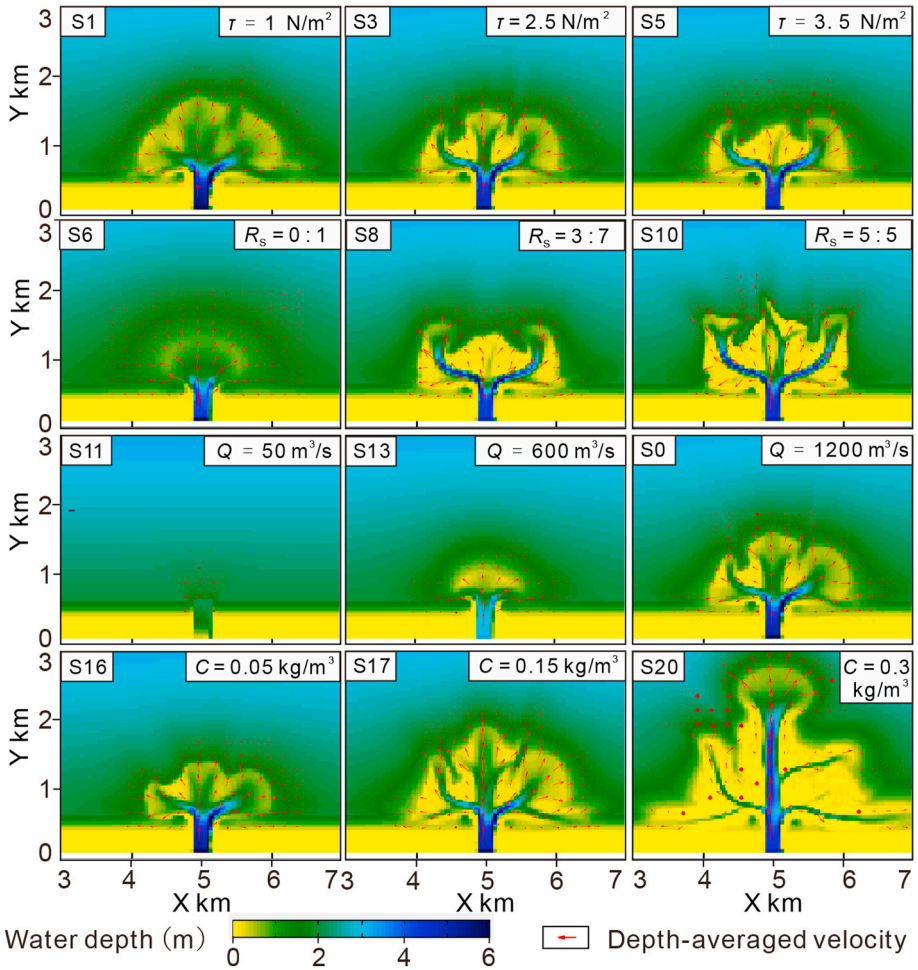

Fig. 16. Water depths and depth-averaged velocities at 80 simulated hours under different upstream conditions. *τ*: *critical shear stress for the erosion of cohesive sediments*; R_S: sand proportion; *Q*: *water discharge*; *C*: *sediment concentration*.

positively scales with water discharge, but they didn't consider the effect of sediment supply. For sinuous bar fingers, high water discharge provides the strong centrifugal force of water flow, which promotes avulsions and then increases the number of bar fingers after the same growth time. However, if considering the same sediment supply, high water discharge doesn't have an evident influence on the number of bar fingers.

6.3. Application to a digitate shallow-water delta reservoir

Digitate shallow-water delta reservoirs have been explored in many petroliferous basins (e.g., Ordos Basin: Hu et al., 2008; Bohai Bay Basin: Zhang et al., 2017; Xu et al., 2019). The sandy bar fingers were the targets, with widths corresponding to only 1–2 folds of well space. Therefore, it is difficult to predict the morphologies (e.g., width and sinuosity) of bar fingers and their distributary channels based on well data. The empirical equations in this paper provide a method of predicting morphology based on the upstream conditions and, in turn, improve the predictability of the inter-well uncertainty in digitate shallow-water delta reservoirs.

Here, we use the digitate shallow-water reservoir in BZ25 Oilfield as an example to demonstrate the application of empirical equations. BZ25 Oilfield is located in Southern Bohai Bay, China, tectonically near Bozhong Sag and Huanghekou Sag (Sun et al., 2011; Jia et al., 2005; Meng et al., 2016) (Fig. 17A and B). The shallow-water reservoir formed in the Lower Member of the Minghuazhen Formation, Neogene, with a buried depth of 1300–1900 m and consists of Oil Groups I–VI (Xu et al., 2019). The bar fingers are 200–500 m wide, as determined using high-frequency seismic data (Fig. 17C). Distributary channel and mouth bar deposits exhibit different recovery efficiencies and remnant oil distributions (Xu et al., 2019). However, seismic data cannot distinguish distributary channel deposits from mouth bars in bar fingers, and well data (well spacing is ~200 m) are not sufficient to predict the inter-well distributions of distributary channels. We estimate that: basinal water depth is < 10 m (based on mouth bar thickness in well); distributary channel depth is also <10 m; The ratio of distributary channel depth to basinal water depth is ~1.0–1.3 (based on the ratio of distributary channel thickness and mouth bar thickness in well); wave and tidal energies are weak (based of the lack of related sedimentary structures in cores). Therefore, this digitate shallow-water delta has similar downstream conditions (similar ratio of distributary channel depth to basinal water depth and weak wave and tidal energies) with modern deposits and simulations mentioned in this paper, so that empirical equation (6) could be used to predict the average nondimensional width (average width ratio of the bar finger to the distributary channel). We then calculated the average distributary channel width, which is critical to identify the boundary between the mouth bar and distributary channel deposits.

For example, the bar fingers in layer IV4.1 are 400 wide and 9 m thick on average (removing compaction). The channel bankfull depth is approximately 10 m according to channel thickness (removing compaction). The sediment supply was estimated using the 0.9 times of sediment mass (0.9 × area × average thickness × density) because most of the sediments were trapped by fluvial-dominated delta with a sediment trapping efficiency of ~0.9 (Wolinsky et al., 2010). The sediment mass of bar fingers in Fig. 17C is more than 5.0×10^7 t (i.e., nondimensional sediment supply >100%). According to the well data, the estimated sand proportion is approximately 0.4, and the sediment cohesion is approximately 1 N/m^2. The upstream river is a meandering river (Fig. 17B) so the water discharge (Q) can be estimated using (Schumm, 1972)

$$Q = 0.028W^{1.3}\mathrm{D}^{1.13} \tag{11}$$

where W is the channel bankfull width, m, and D is the channel bankfull depth.

Schumm and Khan (1972) established the relationship between the slope and sediment concentration. The basin slope was 0.002, and the sediment concentration (C) could thus be estimated as follows:

$$C = 0.0011W \tag{12}$$

If consider distributary channel bankfull width (W) is nearly average distributary channel width, Based on equations (6), (11) and (12), we obtained the following analytical values: the average nondimensional width of the bar fingers was ~7.0, average distributary channel width was ~55 m, water discharge was ~70 m^3/s, and sediment concentration

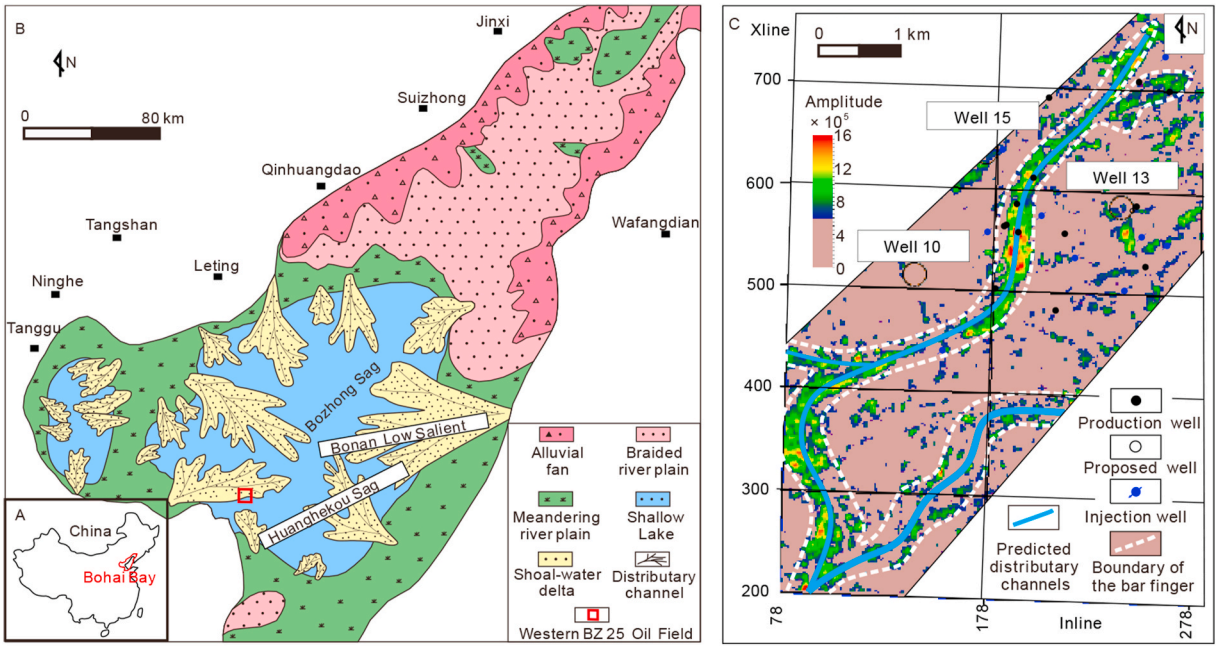

Fig. 17. (A) Location of Bohai Bay in China. (B) Facies and tectonic distribution at the Lower Member of Minghuazhen Formation in Bohai Bay (Deng, 2008; Xu et al., 2019) and location of the western BZ25 Oilfield. (C) Map of the seismic amplitude at IV4.1 layer in the western BZ25 Oilfield. High amplitude (>6 × 10^5) represents the distribution of the digitate shallow-water delta. The white dashed curve is the delta boundary.

was ~0.07 kg/m^3. According to the well data, we predicted the distributary channel distribution (Fig. 17C).

Above analytical values have uncertainties because equations carry uncertainty. Equation (12) was established from laboratory experimental data, hence, we considered that predictive C exhibited enormous uncertainty with a ±50% error, i.e. C = (0.035–0.105) kg/m^3. Although Equation (11) was established from modern deposits, we considered predictive Q with a ±25% error, i.e. Q = (50–90) m^3/s. Predictive nondimensional width of the bar fingers by Equation (6) primarily exhibits a ±10% error according to the examination of modern deposits. Above all, the predicted average distributary channel width in layer IV4.1 was 50–65 m.

7. Conclusions

This study demonstrated the effects of the upstream conditions on digitate shallow-water deltas that develop with similar downstream conditions (basin water depths of a few meters, basin slopes less than 0.1°, and weak wave and tide processes). Digitate shallow-water deltas are characterized by one or multiple separate bar fingers, so we adopted four metrics to quantify the morphological characteristics: the average sinuosity, average nondimensional width (average width ratio of the bar fingers to the distributary channels), nondimensional delta length (ratio between the delta length and average width of the distributary channels), and the number of bar fingers. The values of the metrics have wide ranges and are poorly related to one another.

The 21 Delft3D simulations revealed the quantitative relationships between the morphological metrics and upstream conditions in digitate shallow-water deltas: (1) the average sinuosity has linear relationships with the sediment cohesion and concentration and inverse linear relationships with the sand proportion and water discharge, and reaches equilibrium as sediment supply increases; (2) the average nondimensional width is proportional to the sediment concentration, is inversely proportional to the sediment cohesion and water discharge, and has an inverse exponential relationship with the sand proportion, and is independent of the sediment supply; (3) the delta length has a power-law relationship with the water discharge and is logarithmically related to the sediment supply; and (4) the number of bar fingers is proportional to the sand proportion and sediment supply and inversely proportional to the sediment cohesion.

Using multivariate regression, we established empirical equations for the four aforementioned metrics as functions of the upstream conditions. The empirical equations well predicted the characteristics of nine modern digitate shallow-water deltas and could help improve the prediction of the inter-well uncertainty of the point bar vs. mouth bar in the digitate shallow-water delta reservoirs. However, the empirical equations cannot predict the morphologies of digitate deep-water deltas. Future research on the effects of the downstream conditions will help further reveal the factors controlling the morphological features of bar fingers in digitate deltas.

CRediT author statement

Zhenhua Xu: Conceptualization, Methodology, Software, Visualization, Writing- Original draft preparation. Shenghe Wu: Conceptualization, Writing- Original draft preparation. Dali Yue: Writing- Reviewing and Editing. Junshou Zhao: Investigation. Meng Deng: Resources. Zhao Liu: Investigation. Jiajia Zhang: Software, Investigation. Mingcheng Liu: Validation.

Declaration of competing interest

The authors declare that they have no known competing financial interests or personal relationships that could have appeared to influence the work reported in this paper.

Acknowledgments

The work presented in this paper was financially supported by the National Natural Science Foundation of China (No. 41772101). We thank A. P. Burpee for assistance with the Delft3D simulations. We thank reviewers Andrew Moodie, Helena van der Vegt, Stephan Toby, and other anonymous reviewers, and the Associate Editor Luca Colombera for constructive reviews that significantly improved the manuscript.

References

Aalderink, R.H., Lijklema, L., Breukelman, J., Vanraaphorst, W., Brinkman, A.G., 1985. Quantification of wind induced resuspension in a shallow lake. Water Sci. Technol. 17, 903–914.
Allan, J.C., Kirk, R.M., 2000. Wind wave characteristics at lake Dunstan, south Island, New Zealand. N. Z. J. Mar. Freshw. Res. 34 (4), 573–591.
Baar, A.W., Albernaz, M.B., van Dijk, W.M., Kleinhans, M.G., 2019. Critical dependence of morphodynamic models of fluvial and tidal systems on empirical downslope sediment transport. Nat. Commun. 10 (1), 1–12.
Bagnold, R.A., 1966. An Approach to the Sediment Transport Problem from General Physics. USGS professional paper, 422-I. U.S. Government Printing Office, Washington, D. C.
Bernard, H.A., 1965. A Resume of River Delta Types. AAPG Bulletin, Abstract, p. 49.
Bhattacharya, J.P., Giosan, L., 2003. Wave-influenced deltas: geomorphological implications for facies reconstruction. Sedimentology 50, 187–210.
Burpee, A.P., Slingerland, R.L., Edmonds, D.A., Parsons, D., Best, J., Cederberg, J., McGuffin, A., Caldwell, R., Nijhuis, A., Royce, J., 2015. Grain–size controls on the morphology and internal geometry of river–dominated deltas. J. Sediment. Res. 85, 699–714.
Caldwell, R.L., Edmonds, D.A., 2014. The effects of sediment properties on deltaic processes and morphologies: a numerical modeling study. J. Geophys. Res.: Earth Surf. 119, 961–982.
Caldwell, R.L., Edmonds, D.A., Baumgardner, S., Paola, C., Roy, S., Nienhuis, J.H., 2019. A global delta dataset and the environmental variables that predict delta formation on marine coastlines. Earth Surf. Dynam. 7 (3), 773–787.
Carlson, B., Piliouras, A., Muto, T., Kim, W., 2018. Control of basin water depth on channel morphology and autogenic timescales in deltaic systems. J. Sediment. Res. 88 (9), 1026–1039.
Chaichitehrani, N., Li, C., Xu, K., Allahdadi, M.N., Keim, B.D., 2019. A numerical study of sediment dynamics over sandy point dredge pit, west flank of the Mississippi river, during a cold front event. Continent. Shelf Res. 183, 38–50.
Chung, E.G., Bombardelli, F.A., Schladow, S.G., 2009. Sediment resuspension in a shallow lake. Water Resour. Res. 45 (5), W05422. https://doi.org/10.1029/2007WR006585.
Constantine, J.A., Dunne, T., Ahmed, J., Legleiter, C., Lazarus, E.D., 2014. Sediment supply as a driver of river meandering and floodplain evolution in the amazon basin. Nat. Geosci. 7 (12), 899–903.
Dalrymple, R.W., Choi, K., 2007. Morphologic and facies trends through the fluvial-marine transition in tide-dominated depositional systems: a schematic framework for environmental and sequence-stratigraphic interpretation. Earth Sci. Rev. 81 (3), 135–174.
Deng, Y.H., Li, J.P., 2008. The Formation Process of Shallow Buried Reservoir in Bohai Oilfield. Petroleum Industry Press, Beijing, pp. 50–100 (In Chinese).
Dissanayake, D.M.P.K., Roelvink, J.A., Van der Wegen, M., 2009. Modelled channel patterns in a schematized tidal inlet. Coast. Eng. 56 (11–12), 1069–1083.
Donaldson, A.C., 1966. Deltaic sands and sandstones. 20th Ann. Conf. 31–62.
Donaldson, C.A., 1974. Pennsylvanian sedimentation of central appalachians, 148. Special Paper–Geological Society of America, pp. 47–48.
Dumars, A.J., 2002. Distributary Mouth Bar Formation and Channel Bifurcation in the Wax Lake Delta, Atchafalaya Bay, Louisiana. Louisiana State University, Baton Rouge, p. 88.
Edmonds, D.A., Shaw, J.B., Mohrig, D., 2011. Topset-dominated deltas: a new model for river delta stratigraphy. Geology 39 (12), 1175–1178.
Edmonds, D.A., Slingerland, R.L., 2007. Mechanics of river mouth bar formation: implications for the morphodynamics of delta distributary networks. J. Geophys. Res.: Earth Surf. 112, F04038.
Edmonds, D.A., Slingerland, R.L., 2010. Significant effect of sediment cohesion on delta morphology. Nat. Geosci. 3, 105–109.
Edmonds, D.A., Slingerland, R.L., Best, J., Parsons, D., Smith, N., 2010. Response of river-dominated delta channel networks to permanent changes in river discharge. Geophys. Res. Lett. 37 (12), L12404.
Edmonds, D.A., Paola, C., Hoyal, D.C.J.D., Sheet, B.A., 2011. Quantitative metrics that describe river deltas and their channel networks. J. Geophys. Res. Earth Surf. 116, F04022. https://doi.org/10.1029/2010JF001955.
Falcini, F., Jerolmack, D.J., 2010. A potential vorticity theory for the formation of elongate channels in river deltas and lakes. J. Geophys. Res.: Earth Surf. 115, F04038.
Fisher, W.L., Brown, L.F., Scott, A.J., Mcgowen, J.H., 1969. Delta Systems in the Exploration for Oil and Gas. University of Texas at Austin, Bureau of Economic Geology.
Fisk, H.N., 1954. Sedimentary framework of the modern Mississippi delta. J. Sediment. Petrol. 24, 76–99.

Fisk, H.N., 1955. Sand Facies of Recent Mississippi Delta Deposit. 4th World Petroleum Congress, Rome, Italy, pp. 377–398.
Fisk, H.N., 1961. Bar-finger sands of Mississippi delta. In: Peterson, J.A., Osmond, J.C. (Eds.), Geometry of Sandstone Bodies. American Association of Petroleum Geologists, Tulsa, Okla., pp. 29–52
Galloway, W.E., 1975. Process Framework for Describing the Morphologic and Stratigraphic Evolution of Deltaic Depositional Systems, Deltas: Models for Exploration. Houston Geological Society, Houston, Texas, pp. 87–98.
Geleynse, N., Storms, J.E.A., Walstra, D.J.R., Jagers, H.R.A., Wang, Z.B., Stive, M.J.F., 2011. Controls on river delta formation; insights from numerical modelling. Earth Planet Sci. Lett. 302, 217–226.
Grasmeijer, B., Chu, A., Rijn, L.V., 2011. Application and comparison of two different fine cohesive sediment transport models in Delft3D. Proceed. Coast. Sediments. https://doi.org/10.1142/9789814355537_0132.
Harris, A.D., Covault, J.A., Baumgardner, S., Sun, T., Granjeon, D., 2020. Numerical modeling of icehouse and greenhouse sea-level changes on a continental margin: sea-level modulation of deltaic avulsion processes. Mar. Petrol. Geol. 111, 807–814.
Hofmann, H., Lorke, A., Peeters, F., 2008. Wave-induced variability of the underwater light climate in the littoral zone. Int. Assoc. Theoret.d Appl. Limnol. 30 (4), 627–632.
Hoyal, D.C.J.D, Sheets, B.A., 2009. Morphodynamic evolution of experimental cohesive deltas. J. Geophys. Res. 114 https://doi.org/10.1029/2007JF000882.
Hu, C.H., Qu, H.J., Miao, J.Y., Wang, W.L., Ma, Q., 2008. A study on sedimentary microfacies and oil-bearing possibility in Chang 6 oil-bearing formation in the area of Nanniwan. J. NW Univ. 38 (6), 994–1000.
Huang, Z.W., Xu, X.F., Tang, L.M., Wu, N.H., You, W.S., 2017. Analysis on variation of flow diversion ratio at tail - streams of Ganjiang River. Yangtze River 48 (24), 26–30 +51 (In Chinese).
Hydraulics, WL|Delft, 2003. User Manual Delft3D-FLOW, Delft, Netherlands, p. 686.
Ikeda, S., 1982. Lateral bed load transport on side slopes. J. Hydraul. Div. 108 (11), 1369–1373.
Jerolmack, D.J., 2009. Conceptual framework for assessing the response of delta channel networks to Holocene sea-level rise. Quat. Sci. Rev. 28 (17–18), 1786–1800.
Jerolmack, D.J., Swenson, J.B., 2007. Scaling relationships and evolution of distributary networks on wave-influenced deltas. Geophys. Res. Lett. 34, L23402. https://doi.org/10.1029/2007GL031823.
Ji, Z., Jin, K., 2014. Impacts of wind waves on sediment transport in a large, shallow lake. Lakes Reservoirs Res. Manag. 19 (2), 118–129.
Jia, D., Yang, X., Wu, X., Zhao, L., Zhou, S., 2005. Study of restraining barrier and interbeds in shallow water delta facies controlled by middle well-pattern density-taking Bozhong 25-1 Nan oilfield as example. Petrol. Geol. Recov. Eff. 12 (2), 19–22 (In Chinese).
Kelderman, P., Ang'Weya, R.O., Rozari, P.D., Vijverberg, T., 2012. Sediment characteristics and wind-induced sediment dynamics in shallow lake markermeer, The Netherlands. Aquat. Sci. 74 (2), 301–313.
Kleinhans, M.G., van den Berg, J., 2011. River channel and bar patterns explained and predicted by an empirical and a physics-based method. Earth Surf. Process. Landforms 36 (6), 721–738.
Marfai, M.A., Tyas, D.W., Nugraha, I., Fitriatul'Ulya, A., Riasasi, W., 2016. The morphodynamics of Wulan delta and its impacts on the coastal community in Wedung Subdistrict, Demak regency, Indonesia. J. Environ. Protect. 7 (1), 60–71.
Meng, H., Zhong, D., Li, C., Zhou, J., Qin, G., Liu, Y., Liu, K., 2016. Sedimentary facies and evolution of the member 2 of paleogene Shahejie formation of BZ25-1 oilfield in Bozhong depression, Bohai Bay Basin. J. Paleogeogr. 18 (2), 161–172 (In Chinese).
Milliman, J.D., Farnsworth, K.L., 2013. River Discharge to the Coastal Ocean: a Global Synthesis. Cambridge University Press, pp. 165–330.
Min, Q., 1995. On the regularities of water level fluctuations in Poyang Lake. J. Lake Sci. 7, 281–288 (In Chinese).
Molnar, T.M., 1994. The Birch River: a nonconformable fluvial depositional system in a lacustrine transgressive regime. M. Sc. Thesis. Dept. of Geography, University of Calgary, Calgary, Alberta.
Morton, R.A., Donaldson, A.C., 1978. Hydrology, morphology, and sedimentology of the Guadalupe fluvial-deltaic system. Geol. Soc. Am. Bull. 89 (7), 1030–1036.
Nardin, W., Mariotti, G., Edmonds, D.A., Guercio, R., Fagherazzi, S., 2013. Growth of river mouth bars in sheltered bays in the presence of frontal waves. J. Geophys. Res.: Earth Surf. 118, 872–886.
Nienhuis, J.H., Ashton, A.D., Edmonds, D.A., Hoitink, A.J.F., Törnqvist, T.E., 2020. Global-scale human impact on delta morphology has led to net land area gain. Nature 577 (7791), 514–518.
Olariu, C., Bhattacharya, J.P., 2006. Terminal distributary channels and delta front architecture of river–dominated delta systems. J. Sediment. Res. 76, 212–233.
Olariu, C., Bhattacharya, J.P., Leybourne, M.I., Boss, S.K., Stern, R.J., 2012. Interplay between river discharge and topography of the basin floor in a hyperpycnal lacustrine delta. Sedimentology 59 (2), 704–728.
Orton, G.J., Reading, H.G., 2010. Variability of deltaic processes in terms of sediment supply, with particular emphasis on grain size. Sedimentology 40 (3), 475–512.
Piliouras, A., Kim, W., 2019. Upstream and downstream boundary conditions control the physical and biological development of river deltas. Geophys. Res. Lett. 46 (20), 11188–11196.
Plink-Bjorklund, P., 2012. Effects of tides on deltaic deposition: causes and responses. Sediment. Geol. 279, 107–133.
Postma, G., 1990. An analysis of the variation in delta architecture. Terra. Nova 2, 124–130.
Rowland, J.C., Dietrich, W.E., Stacey, M.T., 2010. Morphodynamics of subaqueous levee formation: insights into river mouth morphologies arising from experiments. J. Geophys. Res.: Earth Surf. 115, F04007.
Schumm, S.A., 1972. Fluvial paleochannels. Soc. Econ. Paleontol. Miner. SP16, 98–107.
Schumm, S.A., Khan, H.R., 1972. Experimental study of channel patterns. Geol. Soc. Am. Bull. 83, 1755–1770.
Schuurman, F., Marra, W.A., Kleinhans, M.G., 2013. Physics-based modeling of large braided sand-bed rivers: bar pattern formation, dynamics, and sensitivity. J. Geophys. Res.: Earth Surf. 118, 2509–2527.
Shankman, D., Keim, B.D., Song, J., 2006. Flood frequency in China's Poyang Lake region: tends and teleconnections. Int. J. Climatol. 26, 1255–1266.
Stouthamer, E., Berendsen, H.J., 2007. Avulsion: the relative roles of autogenic and allogenic processes. Sediment. Geol. 198 (3–4), 309–325.
Sun, H., Zhou, X., Peng, W., Zou, H., Yang, B., He, D., Zeng, X., 2011. Late-stage hydrocarbon accumulation and enrichment in the Huanghekou Sag, southern Bohai Sea. Petrol. Explor. Dev. 38 (3), 307–313.
Syvitski, J.P.M., Saito, Y., 2007. Morphodynamics of deltas under the influence of humans. Global Planet. Change 57 (3–4), 261–282.
Timoney, K., Lee, P., 2016. Changes in the areal extents of the Athabasca river, Birch River, and Cree Creek deltas, 1950–2014, Peace–Athabasca delta, Canada. Geomorphology 258, 95–107.
Van der Vegt, H., Storms, J.E., Walstra, D.J.R., Nordahl, K., Howes, N.C., Martinius, A. W., 2020. Grain size fractionation by process-driven sorting in sandy to muddy deltas. Depositional Rec. 6 (1), 217–235.
Van der Wegen, M., 2009. Modeling Morphodynamic Evolution in Alluvial Estuaries. Ph. D. Thesis. UNESCO-IHE, Delft, the Netherlands.
Van der Wegen, M., Roelvink, J.A., 2012. Reproduction of estuarine bathymetry by means of a process-based model: western Scheldt case study, The Netherlands. Geomorphology 179, 152–167.
Van Rijn, L.C., 1993. Principles of Sediment Transport in Rivers, Estuaries and Coastal Seas. Aqua publications, Amsterdam.
Wang, Z., Liang, Z., 2000. Dynamic characteristics of the Yellow River mouth. Earth Surf. Process. Landforms 25 (7), 765–782.
Wang, J., Muto, T., Urata, K., Sato, T., Naruse, H., 2019. Morphodynamics of river deltas in response to different basin water depths: an experimental examination of the grade index model. Geophys. Res. Lett. 46 (10), 5265–5273.
Wang, Y., Storms, J.E.A., Martinius, A.W., Karssenberg, D., Abels, H.A., 2020. Evaluating alluvial stratigraphic response to cyclic and non-cyclic upstream forcing through process-based alluvial architecture modelling. Basin Res. 1–18, 00.
Wolinsky, M.A., Edmonds, D.A., Martin, J., Paola, C., 2010. Delta allometry: growth laws for river deltas. Geophys. Res. Lett. 37 (21), L21403. https://doi.org/10.1029/2010GL044592.
Wright, L.D., 1977. Sediment transport and deposition at river mouths: a synthesis. Geol. Soc. Am. Bull. 88, 857–868.
Wu, S., Xu, Z., Liu, Z., 2019. Depositional architecture of fluvial-dominated shoal water delta, 02 J. Palaeogeogr. 21, 202–215 (In Chinese).
Xu, D., Xiong, M., Zhang, J., 2001. Analysis on hydrologic characteristics of Poyang Lake. Yangtze. River, 32, 21–27 (In Chinese).
Xu, Z., Wu, S., Liu, Z., Zhao, J., Wu, J., Geng, L., Zhang, T., Liu, Z., 2019. Sand body architecture of the bar finger within shoal water delta front: insights from the lower member of Minghuazhen Formation, Neogene, Bohai BZ25 oilfield, Bohai Bay Basin, east China. Petrol. Explor. Dev. 46, 1–12.
Xu, Z., Plink-Björklund, P., Wu, S., Liu, Z., Feng, W., Zhang, K., Yang, Z., Zhong, Y., 2021. Sinuous bar fingers of digitate shallow-water deltas: insights into their formative processes and deposits from integrating morphological and sedimentological studies with mathematical modelling. Sedimentology. https://doi.org/10.1111/sed.12923.
Yang, M., Wang, G., 1995. The incipient motion formulas for cohesive fine sediments. J. Basic Sci. Eng. 3, 99–109 (In Chinese).
Zhang, J., Wang, M., Wang, Y., Jiang, Y., Lei, Y., Zhang, L., Wang, J., 2017. Identification and sedimentary evolution of the shallow water delta of bird-foot in Bozhong 28-2S oilfield group of Bohai Bay Basin, 09 Period. Ocean Univ. China 47, 77–85 (In Chinese).